Submitted to Physics of Fluids

LBL-8102
Preprint

REALISTIC VLASOV SLAB EQUILIBRIA WITH MAGNETIC SHEAR

Harry E. Mynick, William M. Sharp, and
Allan N. Kaufman

August 1978

Prepared for the U. S. Department of Energy
under Contract W-7405-ENG-48

DISCLAIMER

REALISTIC VLASOV SLAB EQUILIBRIA WITH MAGNETIC SHEAR

Harry E. Mynick, William M. Sharp, and Allan N. Kaufman

Lawrence Berkeley Laboratory
University of California
Berkeley, California 94720

ABSTRACT

A method is described for generating exact Vlasov slab equilibria to model high-beta plasmas with strong magnetic shear. Physically reasonable distribution functions that account for such effects as end losses and density gradients are constructed from constants of the motion and used to calculate the self-consistent electrostatic and magnetic fields. As an application we present numerically calculated equilibria modeling a tormac sheath.

I. INTRODUCTION

Several experimental plasma confinement devices such as tormacs, reversed field mirrors, and tokamaks with poloidal divertors have regions where fields and plasma properties vary strongly normal to flux surfaces. To analyze plasma stability and transport in these regions, it is essential to know the self-consistent equilibrium fields and distribution functions. This paper presents a method for constructing exact Vlasov slab equilibria to model nearly collisionless plasmas with strong cross-field variation.

Most previous work on Vlasov slab equilibria has assumed unsheared magnetic fields.[1-7] Both Holdren[8] and Channell[9] obtain slab equilibria with magnetic shear, but they neglect the electrostatic potential and limit themselves to anlytically tractable distribution functions which are inappropriate for modeling many experimental plasmas. In this paper we introduce a formalism free of these restrictions and use it to construct realistic slab equilibria. Section II presents a general set of equilibrium equations for a collisionless plasma slab. A method is described in section III for constructing physically plausible distribution functions from the constants of the motion, and we discuss calculation of the the corresponding self-consistent fields. This procedure yields exact equilibria without a small-gyroradius expansion. In section IV, we use the method to find equilibria modeling a tormac sheath and present the numerically calculated results.

REALISTIC VLASOV SLAB EQUILIBRIA WITH MAGNETIC SHEAR

Harry E. Mynick, William M. Sharp, and Allan N. Kaufman

Lawrence Berkeley Laboratory
University of California
Berkeley, California 94720

ABSTRACT

A method is described for generating exact Vlasov slab equilibria to model high-beta plasmas with strong magnetic shear. Physically reasonable distribution functions that account for such effects as end losses and density gradients are constructed from constants of the motion and used to calculate the self-consistent electrostatic and magnetic fields. As an application we present numerically calculated equilibria modeling a tormac sheath.

I. INTRODUCTION

Several experimental plasma confinement devices such as tormacs, reversed field mirrors, and tokamaks with poloidal divertors have regions where fields and plasma properties vary strongly normal to flux surfaces. To analyze plasma stability and transport in these regions, it is essential to know the self-consistent equilibrium fields and distribution functions. This paper presents a method for constructing exact Vlasov slab equilibria to model nearly collisionless plasmas with strong cross-field variation.

Most previous work on Vlasov slab equilibria has assumed unsheared magnetic fields.[1-7] Both Holdren[8] and Channell[9] obtain slab equilibria with magnetic shear, but they neglect the electrostatic potential and limit themselves to anlytically tractable distribution functions which are inappropriate for modeling many experimental plasmas. In this paper we introduce a formalism free of these restrictions and use it to construct realistic slab equilibria. Section II presents a general set of equilibrium equations for a collisionless plasma slab. A method is described in section III for constructing physically plausible distribution functions from the constants of the motion, and we discuss calculation of the the corresponding self-consistent fields. This procedure yields exact equilibria without a small-gyroradius expansion. In section IV, we use the method to find equilibria modeling a tormac sheath and present the numerically calculated results.

II. MODEL

We follow Channell in writing the equilibrium field equations in a form appropriate for a slab geometry. A Cartesian frame is chosen with the x-axis in the direction of the plasma spatial variation. Since the electrostatic potential Φ and vector potential $\underset{\sim}{A}$ then depend only on x, they give an electric field $\underset{\sim}{E} = (-\partial\Phi/\partial x, 0, 0)$ and a magnetic field $\underset{\sim}{B} = (0, -\partial A_z/\partial x, \partial A_y/\partial x)$. The gauge is chosen so that $A_x = 0$. In these fields, the constants of the motion for a particle of species s are the Hamiltonian

$$H = \frac{1}{2} m_s (v_x^2 + v_y^2 + v_z^2) + q_s \Phi \tag{2.1}$$

and the y and z components of canonical momentum

$$P_y = m_s v_y + \frac{q_s}{c} A_y$$

$$P_z = m_s v_z + \frac{q_s}{c} A_z \,. \tag{2.2}$$

Here q_s and m_s are the charge and mass of a particle of species s, and $\underset{\sim}{v}$ is particle velocity. Any equilibrium distribution function f_s describing the phase-space distribution of particles of the species can then be written as a function of these invariants alone,[10] and the steady state charge and current densities for the species are appropriate moments of f_s:

$$\rho_s = \frac{q_s}{m_s} \left(\frac{2}{m_s}\right)^{1/2} \int_{-\infty}^{\infty} dP_y \int_{-\infty}^{\infty} dP_z \int_{H_s}^{\infty} dH \, \frac{f_s(P_y, P_z, H)}{(H - H_s)^{1/2}} \tag{2.3}$$

$$\underset{\sim}{j}_s = \frac{q_s}{m_s}\left(\frac{2}{m_s}\right)^{1/2} \int_{-\infty}^{\infty} dP_y \int_{-\infty}^{\infty} dP_z \int_{H_s}^{\infty} dH \, \frac{f_s(P_y,P_z,H)}{(H-H_s)^{1/2}} \left(\underset{\sim}{P} - \frac{q_s}{c}\underset{\sim}{A}\right). \qquad (2.4)$$

Here ρ_s and $\underset{\sim}{j}_s$ are functions of x through the lower bound on H,

$$H_s = \frac{1}{2m_s}\left[\left(P_y - \frac{q_s}{c}A_y\right)^2 + \left(P_z - \frac{q_s}{c}A_z\right)^2\right] + q_s\Phi \, , \qquad (2.5)$$

and f_s is normalized so that integration over velocity space gives the species number density $N_s = \rho_s/q_s$. Total charge and current density are the sums $\rho = \sum_s \rho_s$ and $\underset{\sim}{j} = \sum_s \underset{\sim}{j}_s$. With appropriate boundary conditions, Poisson's equation

$$\frac{d^2\Phi}{dx^2} = -4\pi\rho \qquad (2.6)$$

and Ampere's equation

$$\frac{d^2\underset{\sim}{A}}{dx^2} = -\frac{4\pi}{c}\,\underset{\sim}{j} \qquad (2.7)$$

then determine the self-consistent fields.

The field equations (2.6) and (2.7) are rewritten in a convenient form using expressions for ρ and $\underset{\sim}{j}$ obtained from the momentum conservation equation

$$\underset{\sim}{\nabla}\cdot\underset{\approx}{\Pi} = \rho\underset{\sim}{E} + \frac{1}{c}\,\underset{\sim}{j} \times \underset{\sim}{B} \, , \qquad (2.8)$$

where $\underset{\approx}{\Pi}$ is the pressure tensor. Since the xx component of $\underset{\approx}{\Pi}$, given by

$$\Pi_{xx} = \sum_s m_s \int d^3v\, f_s(\underset{\sim}{v}) v_x^2$$

$$= \sum_s \frac{1}{m_s} \left(\frac{2}{m_s}\right)^{3/2} \int_{-\infty}^{\infty} dP_y \int_{-\infty}^{\infty} dP_z \int_{H_s}^{\infty} dH\, f_s(P_y, P_z, H)\, (H - H_s)^{1/2} \quad , \tag{2.9}$$

is a functional of Φ and $\underset{\sim}{A}$ through H_s, the x component of $\underset{\sim}{\nabla} \cdot \underset{\approx}{\Pi}$ can be rewritten

$$\frac{d\Pi_{xx}}{dx} = \frac{d\Phi}{dx} \frac{\partial \Pi_{xx}}{\partial \Phi} + \frac{d\underset{\sim}{A}}{dx} \cdot \frac{\partial \Pi_{xx}}{\partial \underset{\sim}{A}} = \left(- \frac{\partial \Pi_{xx}}{\partial \Phi}\right) E_x + \left[\left(\frac{\partial \Pi_{xx}}{\partial \underset{\sim}{A}}\right) \times \underset{\sim}{B}\right]_x \quad . \tag{2.10}$$

Comparing (2.10) with the x component of (2.8) then gives the relations

$$\rho = - \frac{\partial \Pi_{xx}}{\partial \Phi} \tag{2.11}$$

and

$$\underset{\sim}{j} = c \frac{\partial \Pi_{xx}}{\partial \underset{\sim}{A}} \quad . \tag{2.12}$$

Introducing the functional $U(\Phi, \underset{\sim}{A}) \equiv 4\pi\, \Pi_{xx}(\Phi, \underset{\sim}{A})$, the field equations (2.6) and (2.7) take the form

$$\frac{d^2\Phi}{dx^2} = \frac{\partial U}{\partial \Phi} \tag{2.13}$$

and

$$\frac{d^2 \underset{\sim}{A}}{dx^2} = - \frac{\partial U}{\partial \underset{\sim}{A}} \quad . \tag{2.14}$$

For any choice of functions f_s and any initial values of Φ, $\underset{\sim}{A}$, and their derivatives, (2.13) and (2.14) may in principle be integrated to give the self-consistent fields as functions of x. Since evaluation

of $U(\underset{\sim}{\Phi},\underset{\sim}{A})$ can be unwieldly in practice, it is often convenient when $\varepsilon \equiv |\rho|/\sum_s |\rho_s| \ll 1$ to calculate $\Phi(\underset{\sim}{A})$ from the quasineutrality condition

$$\frac{\partial U}{\partial \Phi} \approx 0 \ , \tag{2.15}$$

rather than from (2.13). This approximation is equivalent to expanding Φ in powers of ε and solving (2.13) to lowest order. The vector potential may then be calculated from (2.14) using a two-dimensional functional $U(\underset{\sim}{A}) \equiv U[\Phi(\underset{\sim}{A}),\underset{\sim}{A}]$. Redefining U does not change the form of Ampere's equation because

$$\frac{\partial U(\underset{\sim}{A})}{\partial \underset{\sim}{A}} = \frac{d\Phi}{d\underset{\sim}{A}} \frac{\partial U(\Phi,\underset{\sim}{A})}{\partial \Phi} + \frac{\partial U(\Phi,\underset{\sim}{A})}{\partial \underset{\sim}{A}} \approx \frac{\partial U(\Phi,\underset{\sim}{A})}{\partial \underset{\sim}{A}} \tag{2.16}$$

for a quasineutral plasma. When Φ is eliminated in this way, Ampere's equation has the same form as the motion equation of a particle in a two-dimensional potential: Components of $\underset{\sim}{A}$ correspond to spatial coordinates, x is analogous to time, and U may be considered a pseudopotential.

III. CONSTRUCTION OF EQUILIBRIA

Important qualitative features of the equilibrium fields and velocity space distribution functions of a plasma are often known from experiment or physical arguments. We construct Vlasov slab equilibria incorporating these features by a procedure with three principal steps:

a. A physically plausible reference vector potential $\tilde{\underset{\sim}{A}}(x)$ is first chosen, along with an appropriate set of velocity space distribution functions $\tilde{f}_s(x,v_\parallel,v_\perp)$. Here, $v_\parallel$ and $v_\perp$ are the components of particle velocity respectively along and perpendicular to the magnetic field at x.

b. To construct equilibrium distribution functions $f_s(P_y,P_z,H)$ resembling the reference functions $\tilde{f}_s$, we define a generalized guiding center $\tilde{x}_c(P_y,P_z)$ for a particle moving in the reference field $\tilde{\underset{\sim}{A}}$, and equate f_s with $\tilde{f}_s[\tilde{x}_c,\tilde{v}_\parallel(\tilde{x}_c),\tilde{v}_\perp(\tilde{x}_c,H)]$.

c. The pseudopotential $U(\underset{\sim}{A})$ is evaluated for this set of equilibrium distributions, and Ampere's equation (2.14) is then integrated to obtain the self-consistent vector potential. Initial values of $\underset{\sim}{A}$ and $d\underset{\sim}{A}/dx$ in the integration are adjusted to minimize $|\underset{\sim}{A}-\tilde{\underset{\sim}{A}}|$.

Each of these steps will be discussed subsequently. Provided that the calculated self-consistent vector potential approximately matches the reference field $\tilde{\underset{\sim}{A}}$, the equilibrium distribution functions retain the physical features of the reference distributions $\tilde{f}_s$ and give an equilibrium magnetic field resembling $\tilde{\underset{\sim}{B}} = \nabla\times\tilde{\underset{\sim}{A}}$.

The reference distribution functions $\tilde{f}_s(x,v_\perp,v_\parallel)$ are chosen to model prominant physical effects, such as particle losses, density and

temperature gradients, and plasma currents. Since these distributions serve only to simulate important velocity space features, it is unimportant that the local variables x, $v_\perp$, and $v_\parallel$ are not constants of the motion. Differences between $\tilde{f}_s$ and the equilibrium distributions f_s finally calculated arise automatically from the intrinsically self-consistent formalism. The normalizing factor of each $\tilde{f}_s$ and parameters controlling the mean parallel velocity are chosen to make the reference distribution functions consistent with the reference field. We first analytically evaluate the moments of $\tilde{f}_s$ giving the species number density and the contributions of species s to the parallel current density and Π_{xx}:

$$\tilde{N}_s = \int d^3v\, \tilde{f}_s \tag{3.1}$$

$$\tilde{j}_\parallel^s = q_s \int d^3v\, v_\parallel \tilde{f}_s \tag{3.2}$$

$$\tilde{\Pi}_{xx}^s = m_s \int d^3v\, v_x^2 \tilde{f}_s \ . \tag{3.3}$$

For a quasineutral plasma, these quantities must satisfy three conditions. Approximate charge neutrality requires that

$$\sum_s q_s \tilde{N}_s = 0 \ . \tag{3.4}$$

A condition on the total parallel current is obtained from the parallel component of Ampere's equation:[11]

$$\tilde{j}_\parallel \equiv \sum_s \tilde{j}_\parallel^s = \frac{c}{4\pi} \frac{\tilde{B}_z^2}{B} \frac{d}{dx} \left(\frac{\tilde{B}_y}{\tilde{B}_z} \right) , \tag{3.5}$$

where $\tilde{B} \equiv |\tilde{\underset{\sim}{B}}|$. Finally, a pressure balance constraint results from writing

$$\frac{dU}{dx} = \frac{d\Phi}{dx}\frac{\partial U}{\partial \Phi} + \frac{dA_y}{dx}\frac{\partial U}{\partial A_y} + \frac{dA_z}{dx}\frac{\partial U}{\partial A_z}$$

and substituting (2.13) and (2.14):

$$U = 4\pi \sum_s \tilde{\Pi}^s_{xx} = \frac{1}{2}\left\{[\tilde{B}^2(\infty) - \tilde{B}^2] + \left(\frac{d\tilde{\Phi}}{dx}\right)^2\right\} . \qquad (3.6)$$

When arbitrary quantities such as the relative species parallel currents and the relative number density of each ion species are specified, (3.1)-(3.6) can be solved analytically or numerically for the normalizing factors, the self-consistent potential $\tilde{\Phi}$, and parameters governing $\tilde{j}^s_{\|}$ as functions of x. Since integration over velocity phase in (3.1)-(3.3) averages out the lowest order finite gyroradius corrections to $\tilde{f}_s$, this normalization procedure ensures self-consistency to first order in a_s/L, where a_s is a typical ion gyroradius and L is the scale length of field inhomogeneities

$$L \equiv \min\left[E_x\left(\frac{dE_x}{dx}\right)^{-1}, B_y\left(\frac{dB_y}{dx}\right)^{-1}, B_z\left(\frac{dB_z}{dx}\right)^{-1}\right] . \qquad (3.7)$$

The central step in constructing equilibria is making a correspondence between $f_s(P_y,P_z,H)$ and the reference distribution $\tilde{f}_s(x,v_\perp,v_\|)$. We do this by equating f_s with the value of $\tilde{f}_s$ at some point x_c on a particle orbit in the fields $\tilde{\Phi}$ and $\tilde{\underset{\sim}{A}}$, taking for $v_\perp$ and $v_\|$ the velocity components at x_c. The choice of x_c is somewhat arbitrary because any point on the orbit specified by P_y, P_z, and H could be used. We select a point which coincides with the usual

guiding center when $a_s/L \ll 1$. This choice guarantees that the species number density and contributions to $j_{\|}$ and Π_{xx} agree with (3.1)-(3.3) to first order in a_s/L in the small gyroradius limit. To define x_c, we note that the Hamiltonian $H = P_x^2/2m_s + H_s$ is just the Hamiltonian of a particle in a one-dimensional potential H_s. Each trajectory is confined to an x interval where $H > H_s$, and when $a_s/L \ll 1$, a particle oscillates harmonically about a local minimum of H_s. This minimum point corresponds to the usual guiding center of the particle orbit, and since the location depends only on P_y and P_z when the fields Φ and $\underset{\sim}{A}$ are given, it is a suitable choice for the generalized guiding center x_c. Explicitly, we define x_c by the conditions

$$\left(\frac{dH_s}{dx}\right)_{x=x_c} \equiv 0 \tag{3.8}$$

and

$$\left(\frac{d^2H_s}{dx^2}\right)_{x=x_c} > 0 \ . \tag{3.9}$$

When the fields are nonmonotonic or $\underset{\sim}{B}$ is sheared, H_s may have more than one minimum for some P_y and P_z values. In this case, x_c becomes multivalued, and as Fig. 1 illustrates, some particles with the same value of H can then be trapped in separate x intervals. To construct the equilibrium distribution function $f_s(P_y,P_z,H)$ we first use (3.8) and (3.9) with fields $\tilde{\Phi}$ and $\underset{\sim}{\tilde{A}}$ to find the generalized guiding center $\tilde{x}_c$ appropriate for the reference fields. Since (3.8) gives the relation

$$\frac{1}{c}\left(v_y B_z - v_z B_y\right) + \frac{d\Phi}{dx} = 0 \tag{3.10}$$

at the generalized guiding center, the velocity components at $\tilde{x}_c$ are found to be

$$\tilde{v}_{\parallel}^2 = v^2 - \frac{1}{B^2}(\underset{\sim}{v}\times\tilde{\underset{\sim}{B}})^2 = \frac{1}{m_s^2}\left[\left(P_y - \frac{q_s}{c}\tilde{A}_y\right)^2 + \left(P_2 - \frac{q_s}{c}\tilde{A}_z\right)^2\right] - \left(\frac{c}{\tilde{B}}\frac{d\tilde{\Phi}}{dx}\right)^2 \qquad (3.11)$$

and

$$\tilde{v}_{\perp}^{\,2} = \frac{2}{m_s}(H - q_s\tilde{\Phi}) - \tilde{v}_{\parallel}^2 , \qquad (3.12)$$

where all field quantities are evaluated at $\tilde{x}_c$. When $\tilde{x}_c$ is single-valued for some choice of P_y and P_z, we make the identification

$$f_s(P_y,P_z,H) = \tilde{f}_s[\tilde{x}_c(P_y,P_z),\tilde{v}_{\parallel}(P_y,P_z),\tilde{v}_{\perp}(P_y,P_z,H)]. \qquad (3.13)$$

If $\tilde{x}_c$ is multivalued, f_s is taken to be a weighted average of $\tilde{f}_s$ values. Using superscripts to distinguish quantities at the different $\tilde{x}_c$, the form of f_s is

$$f_s(P_y,P_z,H) = \sum_{\alpha} w^{\alpha}\,\tilde{f}_s[\tilde{x}_c^{\alpha}(P_y,P_z),\tilde{v}_{\parallel}^{\alpha}(P_y,P_z),\tilde{v}_{\perp}^{\alpha}(P_y,P_z,H)], \qquad (3.14)$$

where the weighting factors w^{α} are normalized to give $\sum_{\alpha} w^{\alpha} = 1$. Since the contributions to f_s from particles trapped in separate x intervals are independent, these factors may be chosen arbitrarily. We take w^{α} proportional to the difference between H_s at $\tilde{x}_c^{\alpha}$ and the value at the nearest H_s maximum. This choice is mathematically convenient because it yields a continuous and single-valued distribution function.

Normally both the pseudopotential U and the plasma fields must be calculated numerically. To find $\Phi(\underset{\sim}{A})$, the quasineutrality condition (2.15) is first written as

$$\sum_s q_s \int_{-\infty}^{\infty} dP_y \int_{-\infty}^{\infty} dP_z \int_{H_s}^{\infty} dH \frac{f_s(P_y,P_z,H)}{(H-H_s)^{1/2}} = 0, \qquad (3.15)$$

which is a transcendental equation for Φ when $\underset{\sim}{A}$ is given. This type of equation is often efficiently solved by recursive methods[12] or by root-finding techniques such as Newton-Raphson.[13] The specific method of solution chosen will depend on the form of the distribution functions. A straightforward numerical evaluation of (2.9) with $\Phi = \Phi(\underset{\sim}{A})$ then gives $U(\underset{\sim}{A})$, and the self-consistent fields are calculated by numerical integration of Ampere's equation (2.14), using $\underset{\sim}{A}$ and $d\underset{\sim}{A}/dx$ specified at some point x_0 as initial values. Choosing the initial values corresponds physically to specifying the vector potential and magnetic field at x_0. Even though each set of initial values leads to a self-consistent equilibrium $\underset{\sim}{A}$ field, only values for which $\delta_s \equiv |q_s||\underset{\sim}{A}-\tilde{\underset{\sim}{A}}|/m_s c$ is small compared with the species thermal velocity V_s generally yield an equilibrium velocity space distribution function with the physical features modeled by $\tilde{f}_s$. Larger deviations of $\underset{\sim}{A}$ can significantly distort the velocity space loss boundary of the species and alter the number density and parallel current. Since the reference distributions are normalized to give self-consistency in the small gyroradius limit, satisfactory agreement between $\underset{\sim}{A}$ and $\tilde{\underset{\sim}{A}}$ is usually obtained by choosing $\tilde{\underset{\sim}{A}}$ and $d\tilde{\underset{\sim}{A}}/dx$ at x_0 as initial values. Deviation of the calculated $\underset{\sim}{A}$ from $\tilde{\underset{\sim}{A}}$ then results only from nonlocal current and

charge density contributions due to the finite extent of gyration orbits. The self-consistent electrostatic potential associated with any calculated vector potential is found by substituting $\underset{\sim}{A}$ into $\Phi(\underset{\sim}{A})$.

IV. APPLICATION

To illustrate the method of section III, Vlasov equilibria are constructed that model the sheath of a tormac.[14] The poloidal magnetic field of an idealized two-cusp tormac is shown schematically in Fig. 2. Across the sheath the poloidal beta drops from effectively unity on the separatrix to near zero, while the magnetic field direction rotates substantially. Since the sheath thickness is expected to be comparable with typical ion gyroradii and much smaller than the major or minor radii of the plasma, a slab model of the sheath retaining only the spatial variation normal to flux surfaces is an acceptable approximation. A single ion species with $q_i = Z_i e$ is assumed.

The reference vector potential $\tilde{\underset{\sim}{A}}(x)$ is chosen to have the principal qualitative features expected for tormac fields. If z is taken to be the toroidal direction, then the reference magnetic field components have the limits $\tilde{B}_y \to 0$ and $\tilde{B}_z \to B^-$ inside the plasma as $x \to -\infty$ and approach the constant vacuum values B_y^+ and B_z^+ asymptotically as $x \to +\infty$. Also $\tilde{B}$ should increase monotonically with x, because a tormac is an absolute minimum B configuration. A model magnetic field with these features is

$$\tilde{B}_y \equiv -\frac{d\tilde{A}_z}{dx} = \frac{B_y^+}{[1 + \exp(-\alpha x)]^{1/2}}$$

$$\tilde{B}_z \equiv \frac{d\tilde{A}_y}{dx} = \left[(B_z^+)^2 + \frac{(B^-)^2 - (B_z^+)^2}{1 + \exp(\alpha x)}\right], \tag{4.1}$$

where the parameter α controls sheath thickness and $[(B_y^+)^2 + (B_z^+)^2]/(B^-)^2 > 1$ is required. Integrating (4.1) gives the reference vector potential:

$$\tilde{A}_y = \int_0^x dx' \tilde{B}_z(x')$$

$$\tilde{A}_z = \frac{B_y^+}{\alpha} \ln\left\{ \frac{[1+\exp(-\alpha x)]^{1/2} - 1}{[1+\exp(-\alpha x)]^{1/2} + 1} \right\} . \qquad (4.2)$$

Figure 3 shows a typical field configuration with $B_y^+/B_z^+ = 1.0$ and $\tilde{B}(\infty)/\tilde{B}(-\infty) = 2.0$.

Since field lines in a tormac sheath are open, the local velocity space distribution functions of both the electrons and ions are expected to resemble those in mirror devices. Electrons are assumed significantly colder than ions due to their better thermal contact with the device walls. Consequently, the negative electrostatic potential difference $\Delta\Phi$ that develops along field lines to balance electron and ion losses should be a few times the electron thermal energy T_e and small compared with T_i. Since most electrons are electrostatically trapped, a Maxwellian distribution function

$$\tilde{f}_e(x, v_\parallel, v_\perp) = C_e \exp\left[- \frac{m_e}{2T_e} (v_\parallel^2 + v_\perp^2) + \frac{e\Phi}{T_e} \right] \qquad (4.3)$$

is an appropriate and mathematically convenient choice. Ions are trapped along field lines principally by the higher magnetic field strength at the cusps and are assumed to carry all parallel current. To model these features $\tilde{f}_i$ is taken to be a drifting Maxwellian multipled by a cutoff factor that vanishes continuously at the velocity space loss surface separating the trapped and untrapped particles. If R is the ratio of the maximum B along a flux line to the

local value, then particles are trapped when $v_\perp^2 > (v_\parallel^2 - \frac{2q_i\Delta\Phi}{m_i})/(R-1)$, and the distribution function of trapped particles is

$$\tilde{f}_i(x,v_\parallel,v_\perp) = C_i\left[\frac{m_i R}{2}v_\perp^2 + q_i\Delta\Phi - \frac{m_i}{2}(v_\parallel^2 + v_\perp^2)\right] \cdot\exp\left\{-\frac{m_i}{2T_i}\left[(v_\parallel - V_\parallel)^2 + v_\perp^2\right] - \frac{q_i\Phi}{T_i}\right\}, \tag{4.4}$$

where $V_\parallel$ is the velocity of the Maxwellian. Outside the loss boundary, $\tilde{f}_i$ is assumed to be zero. In general, C_i, R, $\Delta\Phi$, and $V_\parallel$ in (4.4) vary with x, while C_e, T_e, and T_i are treated here as constants. To make these distributions consistent with $\tilde{B}$, the normalization equations (3.1)-(3.6) are reduced to a differential equation for $\tilde{N}_i$:

$$\frac{d\tilde{N}_i}{dx} = -\frac{(8\pi e^2 N_i)^{1/2}}{T_e}\left\{2T_i\left(1 + \frac{1}{4R} + \frac{Z_i T_e}{T_i} - \frac{q_i}{R-1}\frac{\Delta\Phi}{T_i}\right)\tilde{N}_i^2 - \frac{\tilde{B}^2(\infty) - \tilde{B}^2}{8\pi}\tilde{N}_i + \frac{1}{(R-1)T_i}\left(\frac{\tilde{B}}{4}\right)^4\left(\frac{\tilde{a}_i}{\tilde{L}_s}\right)^2\right\}^{1/2}, \tag{4.5}$$

where

$$\tilde{a}_i \equiv \frac{m_i c}{q_i \tilde{B}}\left(\frac{2T_i}{m_i}\right)^{1/2}$$

is the local gyroradius of an ion with energy T_i, and

$$\tilde{L}_s \equiv \left[\frac{2}{\pi}\frac{\tilde{B}_z^2}{\tilde{B}^2}\frac{d}{dx}\left(\frac{\tilde{B}_y}{\tilde{B}_z}\right)\right]^{-1}$$

is the local shear length of the reference field. The numerical solution of (4.5) is then used to calculate required quantities in

$\tilde{f}_e$ and $\tilde{f}_i$:

$$C_e = Z_i \tilde{N}_i(x_0) \left(\frac{m_e}{2\pi T_e}\right)^{3/2} \tag{4.8a}$$

$$C_i = \frac{1}{T_i}\left(\frac{m_i}{2\pi T_i}\right)^{3/2} \frac{R^{1/2}}{(R-1)^{3/2}} \left[\frac{\tilde{N}_i}{\tilde{N}_i(x_0)}\right]^{Z_i T_e/T_i} \exp\left[\frac{-q_i}{R-1}\frac{\Delta\Phi}{T_i} + \frac{R}{(R-1)^2}\left(\frac{\tilde{B}}{4}\right)^4\left(\frac{\tilde{a}_i}{\tilde{L}_s}\right)^2\right] \tag{4.8b}$$

$$V_{\|} = \frac{R}{8(R-1)} \frac{B^2}{(2m_i T_i)^{1/2}} \frac{\tilde{a}_i}{\tilde{N}_i L_s} \tag{4.8c}$$

$$\tilde{\Phi} = \frac{T_e}{e} \ln\left[\frac{\tilde{N}_i}{N_i(x_0)}\right] , \tag{4.8d}$$

where $\tilde{\Phi}$ is taken to be zero at the arbitrary point x_0. The requirement that $d\tilde{N}_i/dx$ in (4.5) be real imposes a constraint on $\tilde{a}_i/\tilde{L}_s$:

$$\frac{\tilde{a}_i}{\tilde{L}_s} < \frac{1}{\pi} \frac{\tilde{B}^2(\infty) - \tilde{B}^2}{\tilde{B}^2} \left[\frac{R-1}{2\left(1 + \frac{1}{4R} + \frac{Z_i T_e}{T_i} - \frac{q_i}{R-1}\frac{\Delta\Phi}{T_i}\right)}\right]^{1/2} .$$

This limit on shear length results from the particular form chosen for $\tilde{f}_i$ and is not intrinsic to the method. With C_e, C_i, $V_{\|}$, and $\tilde{\Phi}$ given by (4.8), the equilibrium electron and ion distribution functions are found from (3.14) to be

$$f_e(H) = C_e \exp\left(-\frac{H}{T_e}\right) \tag{4.9}$$

and

$$f_i(P_y, P_z, H) = \sum_\alpha W^\alpha \left[C_i (R-1)(H-H_c) \exp\left(\frac{-H+2\tilde{v}_{\|}V_{\|}-V_{\|}^2}{T_i}\right)\right]_{\substack{x=\tilde{x}^\alpha_x(P_y,P_z) \\ H>H_c}} . \tag{4.10}$$

Here the cutoff energy H_c is defined

$$H_c \equiv q_i\tilde{\Phi} + \frac{1}{R-1}\left(\frac{m_i R}{2}\tilde{v}_{\|}^2 - q_i\Delta\Phi\right), \tag{4.11}$$

and from (3.11) $\tilde{v}_{\|}$ is given approximately by

$$\tilde{v}_{\|}^2 \approx \frac{1}{m_i^2}\left[\left(P_y - \frac{q_i}{c}\tilde{A}_y\right)^2 + \left(P_z - \frac{q_i}{c}\tilde{A}_z\right)^2\right]. \tag{4.12}$$

Neglecting the ion drift term in (3.11) is permissible for the hot ion plasma considered here because

$$\frac{cE_x}{B} \sim Z_i\frac{m_e}{m_i}\frac{V_e^2}{V_i} \ll V_i . \tag{4.13}$$

Since R and $\Delta\Phi$ in f_i remain arbitrary functions of x in this model, fairly realistic models of ion trapping in the sheath may be used, and the sensitivity of the equilibrium fields to these choices is readily tested.

The equilibrium distribution functions (4.9) and (4.10) simplify calculation of the pseudopotential U. Using (2.9), the electron contribution to U is found to be

$$U_e = -4\pi C_e T_e\left(\frac{2\pi T_e}{m_e}\right)^{3/2}\exp\left(\frac{e\Phi}{T_e}\right) . \tag{4.14}$$

The H integral in the ion contribution U_i can likewise be evaluated analytically, giving

$$U_i = \exp\left(-\frac{q_i\Phi}{T_i}\right)\int_{-\infty}^{\infty} dP_y \exp\left[-\frac{1}{2m_iT_i}\left(P_y - \frac{q_s}{c}A_y\right)^2\right]\int_{-\infty}^{\infty} dP_z \exp\left[-\frac{1}{2m_iT_i}\left(P_z - \frac{q_s}{c}A_z\right)^2\right]$$

$$\cdot \sum_\alpha w^\alpha \left\{\mathscr{F}_i \exp\left[\frac{V_\parallel}{T_i}\left(\tilde{v}_\parallel - V_\parallel\right)\right]\right\}_{x=\tilde{x}_c^\alpha(P_y,P_z)}, \tag{4.15}$$

where

$$\mathscr{F}_i = D\left(1 - \frac{2}{3}\lambda\right) \qquad \lambda \leqslant 0$$

$$= D\left\{\left(1 - \frac{2}{3}\lambda\right)\left[1 - \mathrm{erf}(\lambda^{1/2})\right] + 2\left(\frac{\lambda}{\pi}\right)^{1/2}\exp(-\lambda)\right\}. \qquad \lambda \geqslant 0$$

Here the definitions

$$D \equiv 4\pi T_i\left(\frac{2\pi T_i}{m_i}\right)^{3/2} C_i\,(R-1) \tag{4.16}$$

and

$$\lambda \equiv \frac{H_c - H_i}{T_i} \tag{4.17}$$

have been introduced, and $\mathrm{erf}(x) \equiv \frac{2}{\pi^{1/2}}\int_0^x dy \exp(-y^2)$ is the error function. Since $\tilde{x}_c^\alpha$ is in general a complicated function of P_y and P_z, the remaining integrals in (4.15) require numerical evaluation. The choice of distribution functions also allows the quasineutrality condition (2.15) to be rewritten in a convenient form. Equating the derivatives of (4.14) and (4.15) yields, after some manipulation,

$$\phi = \left(\frac{e}{T_e} + \frac{q_i}{T_i}\right)^{-1} \ln\left\{\frac{I(\Phi,\underset{\sim}{A})}{I[0,\underset{\sim}{\tilde{A}}(x_0)]}\right\}. \tag{4.18}$$

where

$$I(\Phi,\underset{\sim}{A}) \equiv \int_{-\infty}^{\infty} dP_y \exp\left[-\frac{1}{2m_iT_i}\left(P_y - \frac{q_s}{c}A_y\right)^2\right]\int_{-\infty}^{\infty} dP_z \exp\left[-\frac{1}{2m_iT_i}\left(P_z - \frac{q_s}{c}A_z\right)^2\right]$$

$$\cdot \sum_\alpha w^\alpha \left\{\mathscr{G}_i \exp\left[\frac{V_\parallel}{T_i}\left(\tilde{v}_\parallel - V_\parallel\right)\right]\right\}_{x\,=\,\tilde{x}_c^\alpha(P_y,P_z)}$$

and

$$\mathcal{G}_i = D(1 - 2\lambda) \qquad \lambda \leqslant 0$$

$$= D\{(1-2\lambda)[1 - \mathrm{erf}(\lambda^{1/2})] + 2\left(\frac{\lambda}{\pi}\right)^{1/2} \exp(-\lambda)\}. \qquad \lambda \geqslant 0.$$

In (4.18) Φ has been taken to be zero for $\underset{\sim}{A} = \tilde{\underset{\sim}{A}}(x_0)$ with x_0 arbitrary. The only Φ dependence of the integral I in (4.18) comes from H_c, and since $|e\Phi| \sim T_e << T_i$ for a hot ion plasma, H_c for typical ions is insensitive to changes in Φ. Consequently, I is weakly dependent on Φ, and a recursive numerical solution of (4.18) for $\Phi(\underset{\sim}{A})$ is practical.

A computer code has been developed to evaluate U and Φ from (4.14), (4.15), and (4.18), and to calculate the self-consistent fields. The functions R and $\Delta\Phi$, the temperature ratio T_e/T_i, and parameters controlling the shear length and asymptotic values of $\tilde{\underset{\sim}{B}}$ are specified initially. For these parameters, $\Phi(\underset{\sim}{A})$ and then $U[\Phi(\underset{\sim}{A}), \underset{\sim}{A}]$ are calculated in dimensionless form on a nonorthogonal grid with one coordinate constant along the curve $\underset{\sim}{A} = \tilde{\underset{\sim}{A}}$ and the other constant along normals to this curve. This nonorthogonal grid is chosen so that U values are calculated only where the pseudopotential is largest. The calculation of the self-consistent vector potential is interactive: The user first enters initial values of x, $\underset{\sim}{A}$, and $\underset{\sim}{B}$ from a keyboard. The code then integrates (2.14) numerically, computing the derivatives by two-dimensional cubic spline interpolation between U values on the nonorthogonal grid, and returns the deviation parameter $\delta \equiv \max(\delta_i/V_i)$ and the final $\underset{\sim}{B}$ value. The user may then change the initial values and rerun the routine, or run an output routine to plot the self-consistent fields, the number density profile, and the ion velocity

space distribution function at selected x values.

Results of a typical equilibrium calculation are shown in Fig. 4. For this example a sheath width $\alpha^{-1} = 1.5\ a_i$ was specified for the reference field, with $\tilde{B}_y/\tilde{B}_z = 1.0$ at $x=\infty$ and $\tilde{B}(\infty)/\tilde{B}(-\infty) = 2.0$. The energy ratio $T_e/T_i = 0.1$ used here is typical for mirror plasmas. The mirror ratio R was assumed to decrease exponentially from 10.0 to 1.2 across the sheath, while $q_i\Delta\Phi/T_i$ varied linearly between -0.25 and -0.35. This choice of spatial dependences for R and $\Delta\Phi$ is arbitrary. Since $\tilde{f}_i$ is normalized to give a parallel current appropriate for $\tilde{B}$, R, and $\Delta\Phi$ principally affect the ion loss boundary, rather than the equilibrium fields. Tests with other dependences confirm that equilibria are insensitive to these functions. The initial values of A and B used here were arrived at by several trials to minimize δ. For this case, $\delta = 0.3$, and the calculated B components in Fig. 4c closely resemble the reference magnetic field of Fig. 3. Some deviation of the calculated vector potential from $\tilde{A}$ occurs because the finite size of gyration orbits causes a lower peak parallel current than that expected from a small gyroradius treatment. This discrepency is found to vanish when $\alpha^{-1} >> a_i$. One weakness of the present method for constructing sheath equilibria is seen in the contour plots of the ion velocity space distribution function of Fig. 5. Since A deviates from $\tilde{A}$, the loss boundary of the equilibrium distribution function is distorted from the loss boundary of $\tilde{f}_i$. This is a mathematical rather than physical effect and can be corrected by iteratively recalculating f_i and U with a larger $V_{||}$. In the small gyroradius limit, a discrepency between A and $\tilde{A}$ shifts $\langle v_{||} \rangle$ by about

$$\Delta\langle v_{\|} \rangle \approx - \frac{q_i \tilde{B} \cdot (\underset{\sim}{A} - \tilde{\underset{\sim}{A}})}{m_i c \tilde{B}}$$

from the value for $\underset{\sim}{A} = \tilde{\underset{\sim}{A}}$. Since $\langle v_{\|} \rangle = (R-1)V_{\|}/R$ for the ion distribution (4.4), changing $V_{\|}$ by about $-\Delta\langle v_{\|} \rangle R/(R-1)$ approximately compensates for the finite gyroradius weakening of parallel current. Figure 6 shows the self-consistent vector potential and the reference field after a single adjustment of $V_{\|}$. In this case $\underset{\sim}{A}$ coincides with $\tilde{\underset{\sim}{A}}$ within 4% at all x values, and after a second adjustment the discrepency is less than 1%.

V. CONCLUSION

The method presented here for constructing Vlasov equilibria to model strongly inhomogeneous slab plasmas is quite general. The field equations (2.13) and (2.14) are exact, and any degree of physical detail may be incorporated into the reference distribution functions $\hat{f}_s$. Consequently, the equilibria may be used to determine the sensitivity of plasma instabilities and transport to particular features of the physical situation.

Even though the method reliably generates realistic slab equilibria, three intrinsic limitations reduce its usefulness:

a. Qualitative understanding of a plasma configuration is needed to make appropriate choices for the reference field and distributions.

b. Equilibria are obtained numerically except in the simplest cases. Important information about the scaling and parametric dependences of results is therefore unavailable, and the equilibria are not readily used in analytic stability calculations.

c. The method does not indicate which equilibria are physically plausible, because the Vlasov model ignores processes like collisions and field fluctuations which determine transport and losses.

To calculate slab plasma equilibria with less guesswork, a more elaborate numerical treatment using Fokker-Planck equations or particle simulation is required.

ACKNOWLEDGEMENTS

We are grateful to Andrew M. Sessler, Herbert L. Berk, and James H. Hammer for useful discussions of the formalism.

This work was supported by the United States Department of Energy.

REFERENCES

[1] H. Grad, Phys. Fluids 4, 1366 (1961).

[2] G. Schmidt, Phys. Rev. 126, 1611 (1962).

[3] B. Bertotti, Ann. Phys. 25, 271 (1963).

[4] J. Hurley, Phys. Fluids 6, 83 (1963).

[5] R. Nicholson, Phys. Fluids 6, 1581 (1963).

[6] A. Sestero, Phys. Fluids 7, 44 (1964).

[7] S. Lam, Phys. Fluids 10, 2454 (1967).

[8] J. P. Holdren, Phys. Fluids 12, 1059 (1969).

[9] P. J. Channell, Phys. Fluids 19, 1541 (1976).

[10] A. J. Lichtenberg, Phase-Space Dynamics of Particles (John Wiley & Sons, Inc., New York, 1969) p. 33.

[11] This form was suggested by H. L. Berk.

[12] E. Isaacson and H. Keller, Analysis of Numerical Methods, (John Wiley & Sons, Inc., New York, 1966), pp. 86-94.

[13] ibid., pp. 97-99.

[14] C. C. Gallagher, L. S. Combes, and M. A. Levine, Phys. Fluids 13, 1617 (1970).

FIGURE CAPTIONS

Fig. 1. Particles are confined to x intervals where $H \geqslant H_s$. For $H = H_1$ or $H = H_3$ a single region is accessible, whereas a particle with $H = H_2$ can be trapped in either of two distinct intervals.

Fig. 2. Poloidal magnetic field of an idealized two-cusp tormac. The plasma excludes poloidal flux from the shaded interior region, and field lines are toroidal. Outside, the poloidal field increases rapidly across a thin sheath.

Fig. 3. Reference fields $\tilde{\underset{\sim}{A}}$ and $\tilde{\underset{\sim}{B}}$. a) Components of $\tilde{\underset{\sim}{A}}$ vs x.
b) Components and magnitude of $\tilde{\underset{\sim}{B}}$ vs x.

Fig. 4. Equilibrium $\underset{\sim}{A}$ and $\underset{\sim}{B}$ fields. a) Components of $\underset{\sim}{A}$ and $\tilde{\underset{\sim}{A}}$.
b) Components of $\underset{\sim}{A}$ vs x. c) Components and magnitude of $\underset{\sim}{B}$ vs x.

Fig. 5. Reference and equilibrium ion distribution functions $\tilde{f}_i$ and f_i. f_{max} is the local maximum value of $\tilde{f}_i$ or f_i normalized to unity at $x = -\infty$. Dotted lines are contours of constant distribution function at equally spaced values between zero and f_{max}. Solid lines indicate loss boundaries. a) $x = -4.0\ a_i$.
b) $x = 0.0$. c) $x = 4.0\ a_i$.

Fig. 6. Equilibrium $\underset{\sim}{A}$ field after one adjustment of $V_{\|}$.

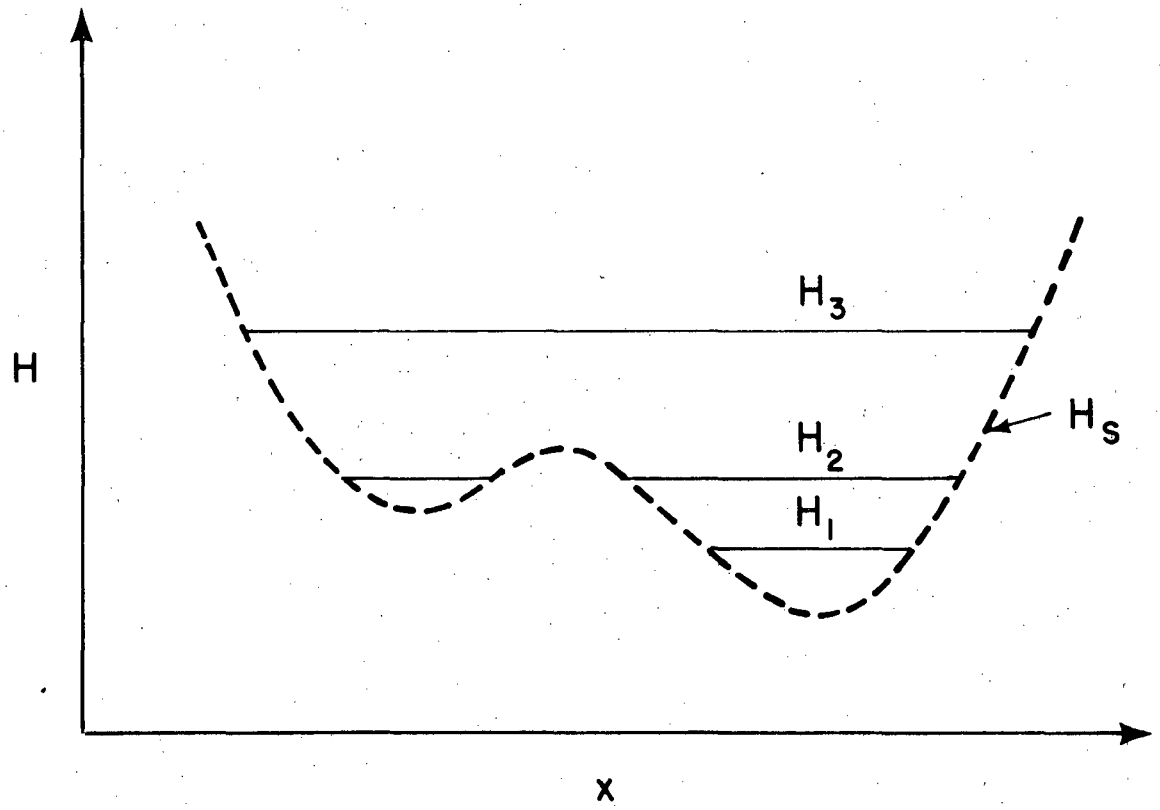

XBL788-1547

Figure 1. Mynick, et al.

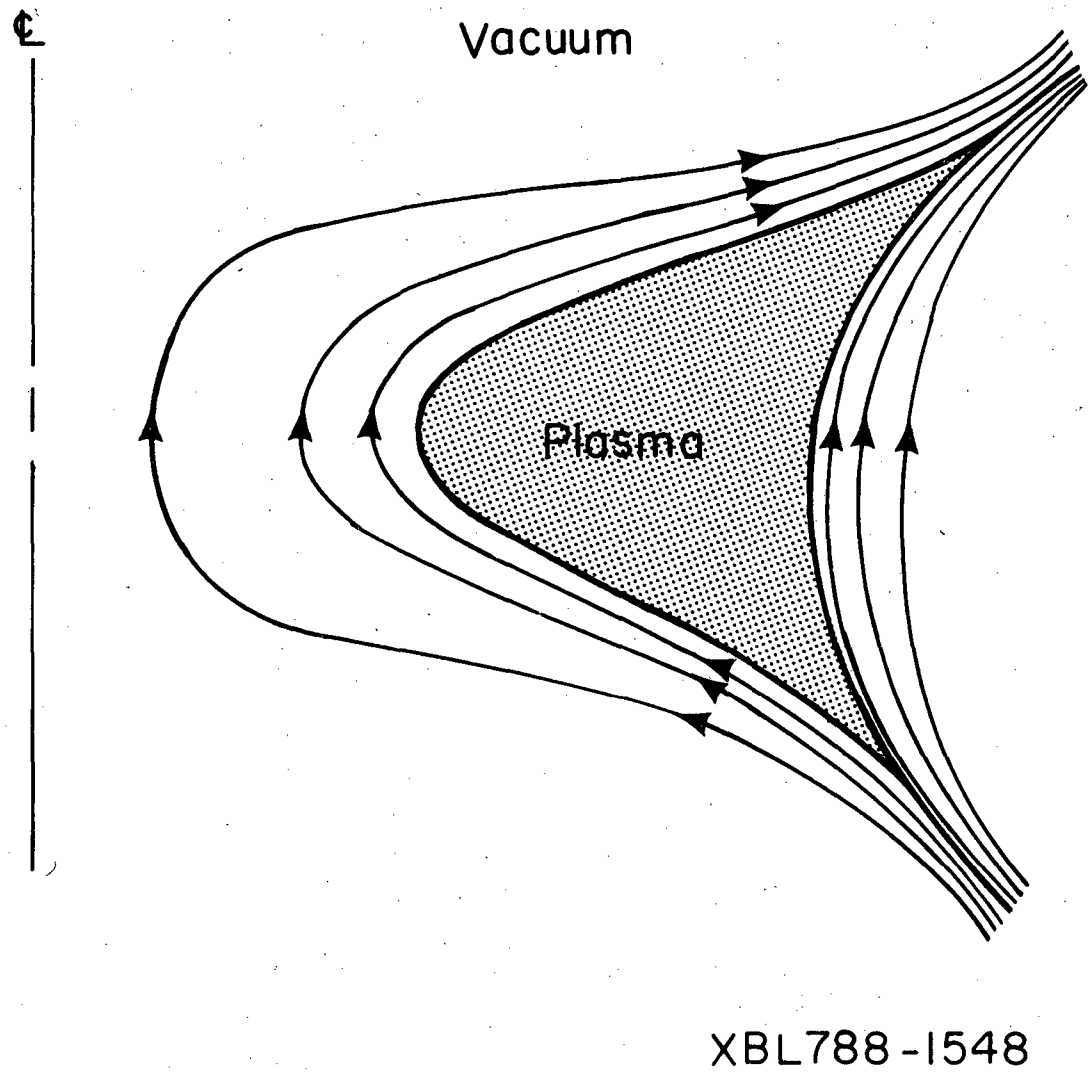

Figure 2. Mynick, et al.

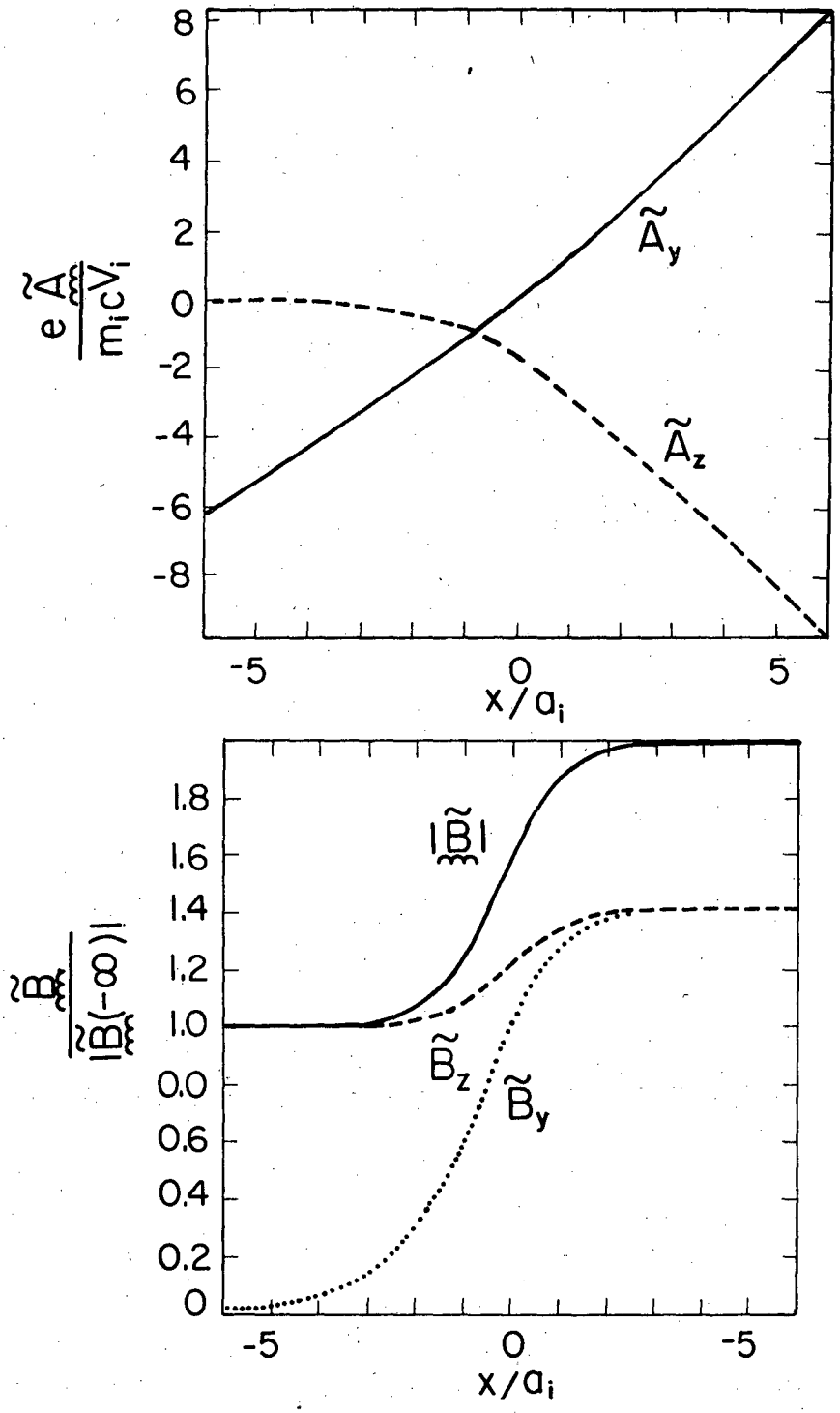

XBL 788-1549

Figure 3. Mynick, et al.

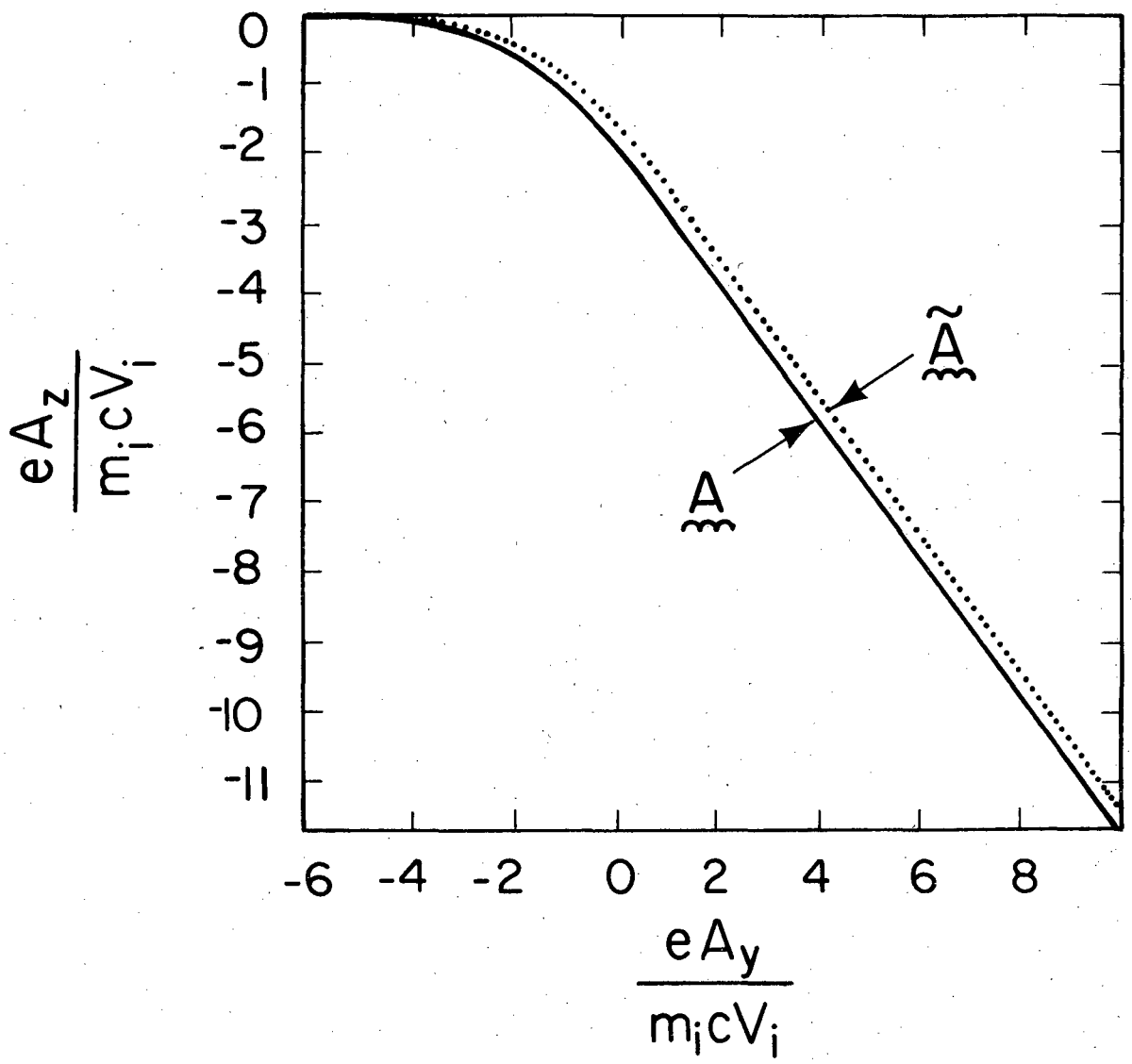

Figure 4a. Mynick, et al.

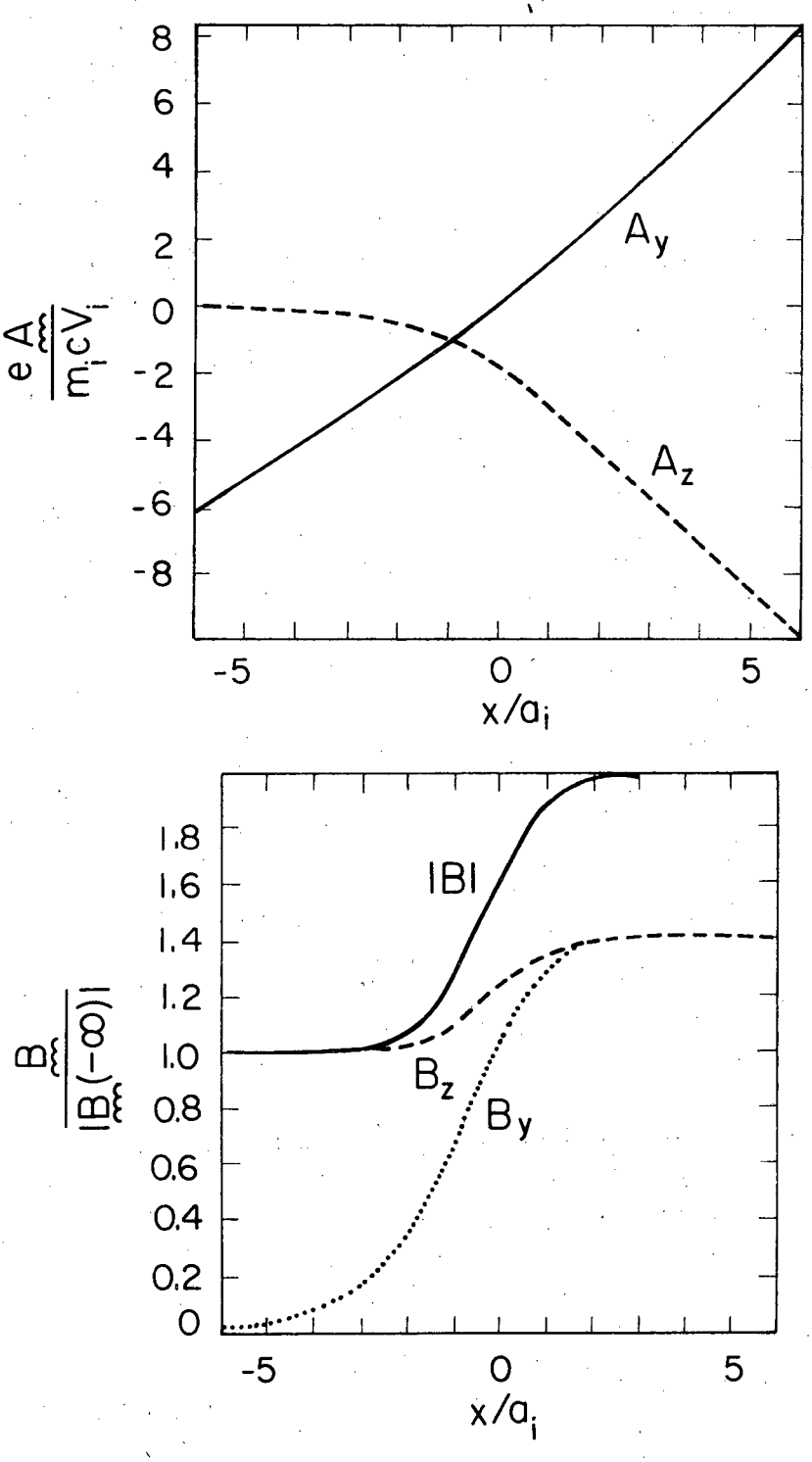

XBL788-1551

Figure 4b, c. Mynick, et al.

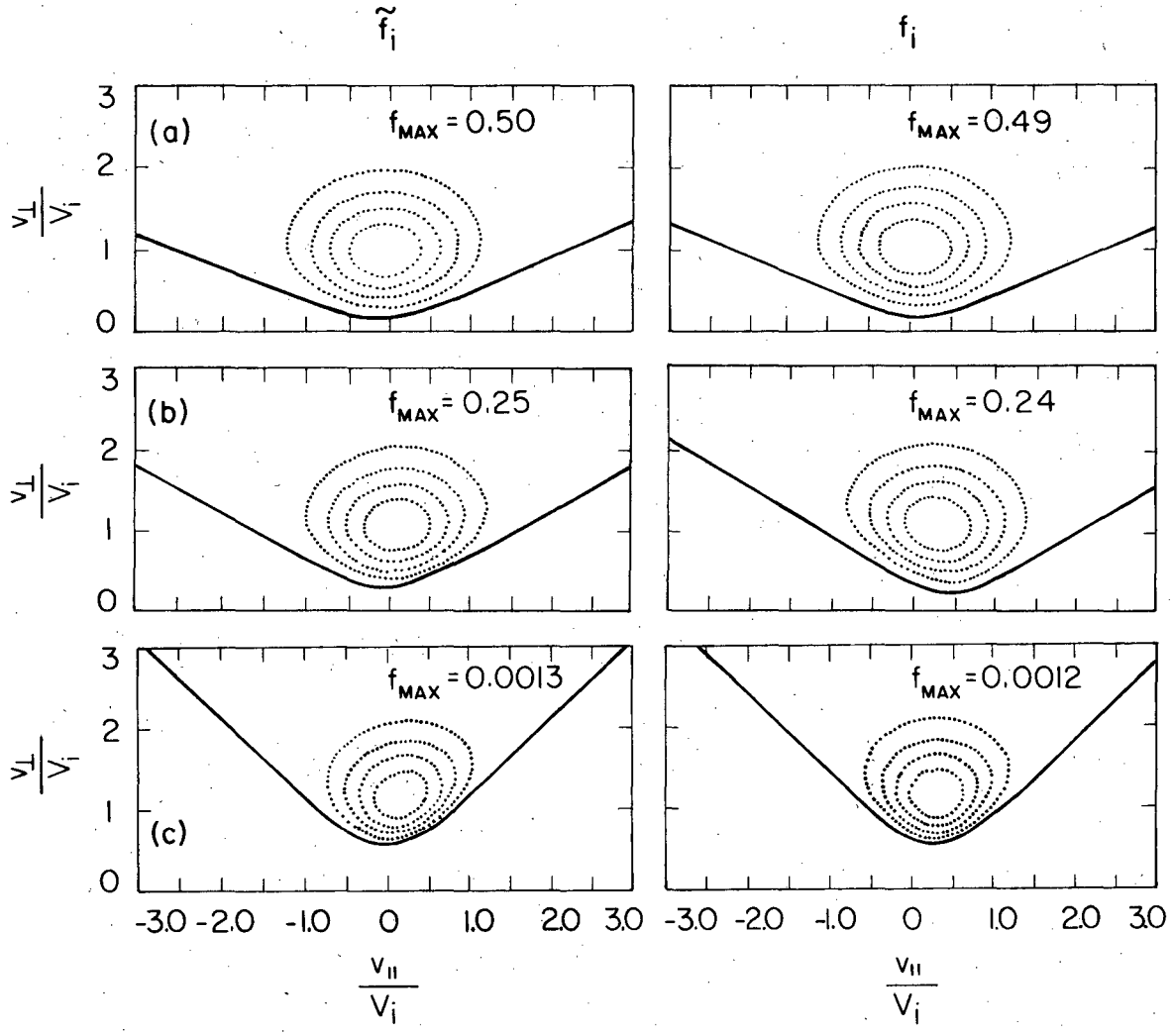

XBL788-1553

Figure 5. Mynick, et al.

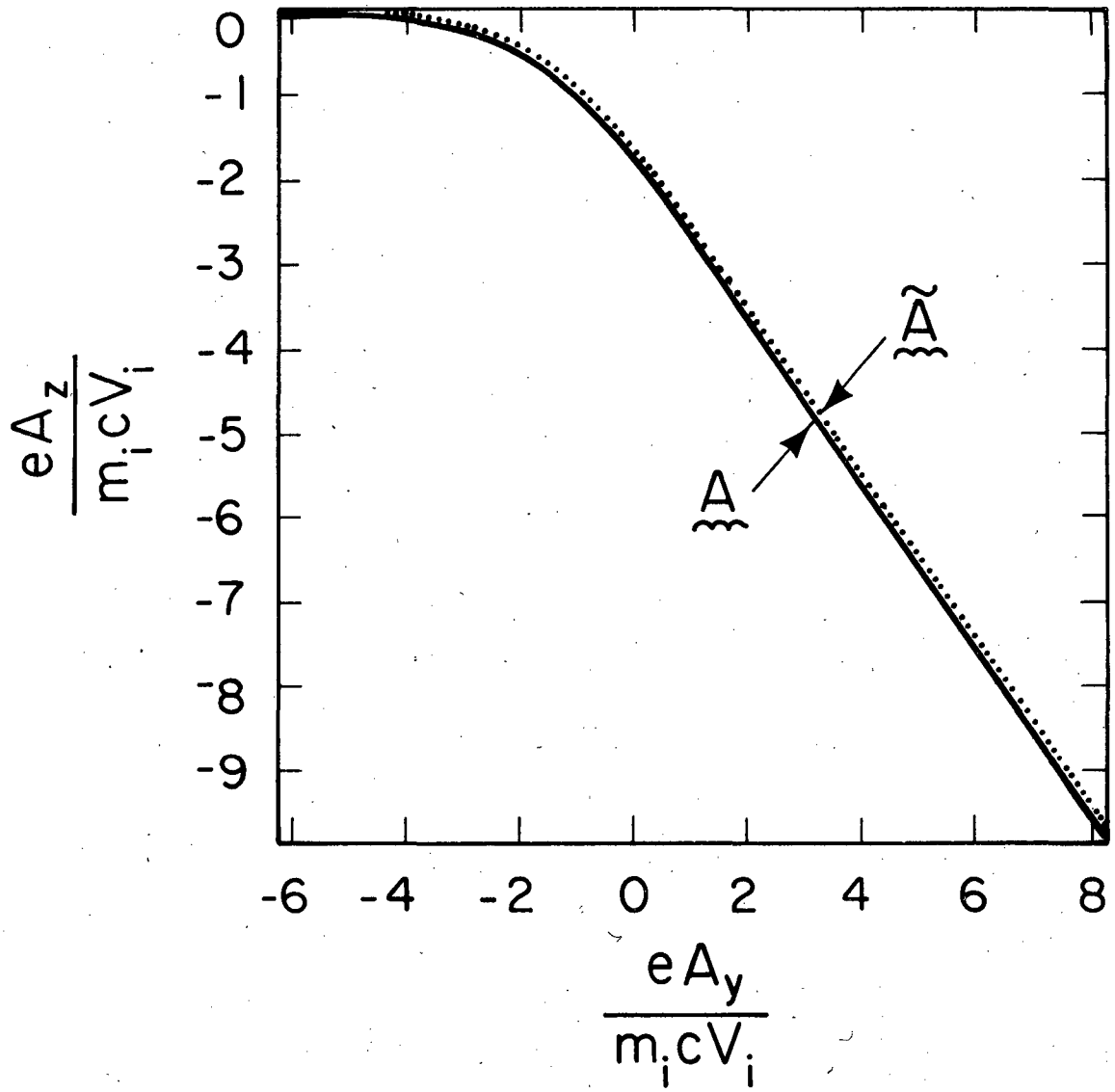

XBL788-1552

Figure 6. Mynick, et al.

TECHNICAL INFORMATION DEPARTMENT
LAWRENCE BERKELEY LABORATORY
UNIVERSITY OF CALIFORNIA
BERKELEY, CALIFORNIA 94720